Journal of Translational Medicine

RESEARCH

Open Access

Single-cell and bulk transcriptome analysis reveals tumor cell heterogeneity and underlying molecular program in uveal melanoma

Ke Li[1,2], Jingzhe Huang[1,2], Ying Tan[1,2], Jie Sun[1,2*] and Meng Zhou[1,2*]

Abstract

Background Uveal melanoma (UM) is a rare and deadly eye cancer with high metastatic potential. Despite the predominance of malignant cells within the tumor microenvironment, the heterogeneity and underlying molecular features remain to be fully characterized.

Methods We analyzed single-cell transcriptomic profiling of 37,660 malignant cells from 17 UM tumors**.** A consensus non-negative factorization algorithm was used to decipher transcriptional programs underlying tumor cell-intrinsic heterogeneity. Tumor-infiltrated immune cells were computationally estimated from bulk transcriptomes and bioinformatics methods. A gene signature was derived for subtyping and prognostic stratification and validated in multicenter cohorts.

Results ScRNA-seq analysis revealed the existence of diverse subpopulations and transcriptional variability among malignant cells within and between tumors. Furthermore, we observed that the heterogeneity of malignant cell states and compositions correlated with genomic, immunological, and clinical characteristics. By identifying gene expression programs associated with malignant cell heterogeneity at the single cell level, UM samples were classified into two distinct intra-tumoral subtypes (ITMH^{lo} and ITMH^{hi}) with different prognoses and immune microenvironments. Finally, a machine learning-derived 9-gene signature was developed to translate single-cell information into bulk tissue transcriptomes for patient stratification and was validated in multicenter cohorts.

Conclusions Our study provides insight into understanding the intra-tumoral heterogeneity of UM and its potential impact on patient stratification.

Keywords Uveal melanoma, Single-cell RNA sequencing, Intra-tumoral heterogeneity

Background

Uveal melanoma (UM) is a rare intraocular malignancy that arises from the melanocytes in the uveal tract of the eye and is the most common primary eye cancer in adults [1, 2]. UM is a relatively rare but deadly cancer with a 1-year overall survival of approximately 50% in metastatic patients [3, 4]. Although the most commonly used first-line treatment options, such as surgery, radiotherapy and enucleation, have improved local disease control of primary tumors, almost 50% of UM patients eventually develop metastases with no or limited curative treatment to improve survival [5, 6].

*Correspondence:
Jie Sun
suncarajie@wmu.edu.cn
Meng Zhou
zhoumeng@wmu.edu.cn
[1] State Key Laboratory of Ophthalmology, Optometry and Visual Science, Eye Hospital, Wenzhou Medical University, Wenzhou 325027, China
[2] National Clinical Research Center for Ocular Diseases, Eye Hospital, Wenzhou Medical University, Wenzhou 325027, China

The clinical challenges posed by UM highlight the need to understand the complex behavior of this tumor. As a hallmark of tumor evolution and progression, intratumoral heterogeneity (ITH) has previously been recognized as a common feature of most solid tumors, but also exhibited cancer type-specific patterns [7–11]. Single-cell technologies have provided unprecedented opportunities to decipher tumor heterogeneity at the cellular level, revealing molecular and phenotypical heterogeneous cancer cell populations within individual tumors at unprecedented depth in several cancer types [12–15]. Emerging evidence has indicated that tumor cell ITH and its complex crosstalk with other critical cellular components of the tumor microenvironment (TME) is a crucial mechanism underlying tumor development, progression, metastasis and occurrence, and contributes to patient prognosis, treatment response, and drug resistance [14, 16–18], thus posing a significant clinical challenge for effective and personalized cancer patient management. However, the ITH of cancer cells at the single-cell level and its impact and clinical implications for UM remain largely uncharacterized.

Here, we performed an integrated analysis of single-cell RNA sequencing (scRNA-seq) and bulk transcriptome to characterize intratumoral diversity and heterogeneity of UM malignant cells, and further underlined their correlations with molecular, biological and clinical features in large patient cohorts. Finally, we identified a gene signature involved in malignant cell heterogeneity that refines the clinically distinct intrinsic subtypes of UM using machine learning. Our study shed insights into the multicellular ecosystem of UM and would have implications for risk stratification and personalized treatment.

Materials and methods

Single-cell transcriptome data and analysis

ScRNA transcriptome data (10X Genomics) from 17 patients were collected from Durante et al. [19] and Pandiani et al. [20] under the accession numbers GSE139829 and GSE138665 in the Gene Expression Omnibus (GEO).

The scRNA-seq data were processed and analyzed using the Seurat R package (v4.0.0) [21]. Unless otherwise stated, functions are executed using default parameters. The scRNA-seq data of all 17 UM patients from two cohorts were integrated into an aggregate Seurat object using the merge function of the Seurat package. High-quality cells with > 200 genes detected and less than 10% of transcripts derived from mitochondria were selected for further analysis. To remove doublet events in the scRNA-seq data, the DoubletFinder R package (v2.0.3) was used to identify 1681 doublets (3.1% doublet rate). The SCTransform method was used to perform normalization and variance stabilization of scRNA-seq datasets with regression for mitochondrial content. A total of 3000 highly variable genes were generated after ranking by residual variance of each gene, and used to perform PCA dimension reduction. The first 30 significant principal components were further summarized to construct SNN graph clustering (resolution = 2) to identify distinct cell clusters, which were illustrated using t-distributed Stochastic Neighbourhood Embedding (t-SNE). Batch effects between patients were minimized using the harmony method in the Harmony R package (v1.0) [22]. We defined the identity of each cell cluster according to the expression of well-known cell markers: Tumor cells (MLANA, MITF), T/ NK cells (CD3D, CD3E), B/ plasma cells (MS4A1, CD38, SDC1), myeloid cells (C1QA, CD14, CD68), Fibroblasts (DCN, C1R, C1S), Endothelial cells (PECAM1, CLDN5, CD34), Photoreceptor cells (RCVRN). Differentially expressed genes (DEGs) between major cell types were identified using the FindAllMarkers function in Seurat with the Wilcoxon rank sum test and Bonferroni correction, and DEGs with log2(fold change) > 0.58 and FDR < 0.05 were retained.

Scoring of T cell properties

The exhaustion, immunosuppression and cytotoxicity signatures for quantifying T-cell properties were collected from Zheng's study [23]. We evaluated the signature scores for each T cell using the AddModuleScore function in Seurat.

Pseudotime trajectory analysis

Monocle (v2.16.0) R package was used to analyze the cellular trajectory to discover the state transitions of tumor cells [24]. The reduceDimension function was used to reduce dimensions using the DDRTree method. Results were visualized in two-dimensional space using the plot_cell_trajectory function and annotated with pseudotime.

SCENIC analysis

SCENIC analysis was performed using the SCENIC R package (v1.2.2) to reconstruct the gene regulatory network [25]. The count matrix from Seurat was imported and filtered with the defined threshold (minCountsPerGene = 0.03 * ncells and minSamples = 0.01* ncells). Potential TF targets were identified using GENIE3 and GRNBoost methods with hg19-500 bp-upstream-7species.mc9nr.feather and hg19-tss-centered-10 kb-7species.mc9nr.feather cisTarget databases. TF activities and active TFs were determined by AUCell.

CNV estimation from scRNA-seq

Copy number variations (CNVs) of tumor cells for each UM sample were inferred from scRNA-seq data using

InferCNV (v1.4.0; https://github.com/broadinstitute/inferCNV). The count matrix from Seurat was imported. To obtain high-quality T cells (non-malignant cells) as baselines to infer the CNVs of tumor cells, only T cells without expression of MLANA, PMEL, MITF and DCT were considered. The cutoff was set to 0.1 and other parameters were default values. To define genomic heterogeneity, we first calculated the CNV score of each tumor cell by the quadratic sum of CNV region—1, and then we averaged the CNV score of tumor cells for each patient to represent the genomic heterogeneity of UM patients.

Bulk transcriptome data and analysis

Bulk RNA-seq data of 80 UM tumors and corresponding clinicopathological information were downloaded from UCSC Xena (GDC TCGA-UM cohort) (https://xenabrowser.net/datapages/). Gene expression levels were normalized to FPKM values and transformed log2(fpkm + 1). Three bulk microarray data of 120 UM tumors and corresponding clinicopathological information were retrieved from GEO, including 63 samples from Laurent's study (accession number GSE22138) [26], 29 samples from Gangemi's study (accession number GSE27831) [27] and 28 samples from van Essen's study (accession number GSE84976) [28]. Raw microarray data profiling by Affymetrix Human Genome U133 Plus 2.0 Array was normalized with the Robust Multichip Average (RMA) method. Processed gene expression data based on Illumina HumanHT-12 V4.0 expression beadchip were provided [27].

Genomic mutation analysis

Somatic mutations and copy number alterations (CNAs) of UM tumors were downloaded from TCGA (https://portal.gdc.cancer.gov/). Significant amplification or deletion of genes was identified using GISTIC 2.0 algorithm with q values < 0.2 based on CNV data in the TCGA-UM cohort [29]. The landscape of CNV patterns and statistically significant cytobands was visualized using the Integrative Genomics Viewer (IGV) [30]. The fraction of genome altered (FGA) was calculated by adding the length of specified copy-number segments (|values| > 0.1) and then dividing by the genome length covered.

Deciphering transcriptional programs underlying tumor cell-intrinsic heterogeneity

We applied a consensus non-negative matrix factorization (NMF) algorithm to decipher transcriptional programs underlying tumor cell-intrinsic heterogeneity from 17 UM samples [31]. For each sample, we first filtered genes (expressed < 5% tumor cells) and low-quality cells (< 1000 genes/cell) and applied NMF to each expression count matrix. We set k = 3:10 as the factor number and selected the optimal k value for each patient, which effectively decomposed the expression matrix. A total of 88 signatures were identified in 17 tumors. To investigate the common features among these signatures, we calculated the Pearson correlation coefficients according to the cell scores of each signature and then clustered them into common programs using hierarchical clustering, which revealed five prevalent expression programs in UM tumors. For each common program, we combined the top 100 genes of each signature in this program, and then calculated the average loadings of each gene. We kept the original loadings for each unique gene and added the total loadings for duplicated genes. For each gene, we divided the loading by the gene number of this program. Finally, the top 30 genes ranked by loadings were defined as the signature of this expression program. We evaluated the program enrichment degree in each tumor cell based on the program signatures using the AddModuleScore function in Seurat.

Cell–cell communication analysis

The cell–cell communication network was inferred from scRNA-seq data using the CellChat R package (v1.1.1) according to canonical ligand-receptor pairs [32].

Computational estimation of tumor-infiltrated immune cells from bulk transcriptomic data

The composition of tumor-infiltrating immune cells was estimated computationally from bulk transcriptomic data using CIBERSORT in the IOBR R package (v0.99.9) and ssGSEA [33].

Identification of ITMH-related DEGs

ITMH-related DEGs were identified for malignant cells between $ITMH^{hi}$ and $ITMH^{lo}$ tumors using the FindMarkers function in the Seurat R package with the Wilcoxon Rank Sum test and Bonferroni correction. DEGs were filtered using the following criteria: the gene expressed in at least 60% of cells in the more abundant group; log2(fold change) > 0.58 and FDR < 0.05.

Generation of a 9-gene signature for tumor cell-intrinsic subtype determination

To develop a clinically applicable gene expression signature, we conducted the multistep analysis as follows: (1) univariate Cox proportional hazards regression for overall survival was used to examine the prognostic value of each ITMH-related DEG, and only $ITMH^{lo}$-specific genes with a hazard ratio < 1 or $ITMH^{hi}$-specific genes with a hazard ratio > 1 were retained for further analysis; (2) When two genes showed a high correlation (> 0.8), we assessed the mean absolute correlation of each gene and eliminated the gene with the highest mean absolute

correlation, and performed feature selection for above-selected genes via recursive feature elimination method. The external resampling method was set to "CV", with the returnResamp parameter set to "final"; (3) Identify valuable features using XGBoost, and train an XGBoost classifier for subtype determination in the TCGA-UM cohort, which was validated in multicenter independent cohorts. Parameters were set as eta = 0.3, max_depth = 10, and the maximum number of boosting iterations was set to 1000.

Statistical analysis

All statistical analyses were performed in R (v4.0.3) on the R studio interface (v1.3.959). Wilcoxon rank sum test or Kruskal–Wallis test was used to compare differences between groups. Univariate and multivariate Cox proportional hazard regression models were used to determine the association between variables and survival. The Kaplan–Meier method and the log-rank test were used to calculate survival differences between different subtypes. Hazard ratios (HR) with 95% confidence intervals (CI) and p values for each variable were visualized using the forestplot R package (v1.10.1).

Results

ScRNA-seq analysis revealed transcriptional heterogeneity of malignant cells within and between UM tumors

Our study incorporated scRNA-seq data of 17 UM tumors from two cohorts. After quality control and doublet removal, 51464 high-quality single cells were retained for subsequent analyses. After principal component analysis and batch effect correction, t-SNE visualization revealed that single-cell transcriptomes from different patients were intermixed, indicating minimal batch effects (Supplementary Fig. 1a). To uncover the cellular composition of UM, we clustered and identified seven major cell types, including malignant cells, photoreceptor cells, endothelial cells, fibroblasts, T/NK cells, B/plasma cells and myeloid cells, based on their canonical cell marker genes (Fig. 1a–c). We conducted differential expression analysis and Spearman's correlation to identify the relationship between clusters based on their top 10 cluster-specific genes. Our results revealed several association groups that were consistent with our annotation findings (Fig. 1d). Notably, all malignant clusters demonstrated a high degree of similarity, but were divided into different submodules, indicating the transcriptional diversity of malignant cells. To further investigate this heterogeneity, we analyzed the transcriptomes of 37,660 malignant cells and categorized them into 19 clusters (Fig. 1e). Interestingly, although patient-specific malignant cells were observed, malignant cells from the same patient were also mapped into different malignant cell subclusters, implying the intratumoral transcriptomic heterogeneity of malignant cells within the same tumor (Fig. 1f–g). We used the diversity score proposed by Ma et al. (13) to quantify the ITH of malignant cells in the TME for a sample. We respectively imported different PCAs as input for the calculation and found that the number of PCAs had little effect on the patient ranking of the diversity scores (Supplementary Fig. 1b), indicating the robustness and reliability of the diversity scores. We then divided 17 patients into two groups with high ($ITMH^{hi}$ tumors, n=8) and low intratumoral malignant cell heterogeneity ($ITMH^{lo}$ tumors, n=9) using the median diversity scores as the cutoff. ITMHhi tumors had significantly higher diversity scores than ITMHlo tumors (Wilcoxon test, p = 8.2e-05) (Supplementary Fig. 1c). These two subtypes corresponded to different clinical behaviors, with ITMHhi tumors exhibiting larger tumor diameter, mixed histopathological features, GEP class 2 subtype and higher metastatic risk (Supplementary Fig. 1d). Furthermore, t-SNE plots at both single-cell and patient level revealed a distinct distribution of $ITMH^{hi}$ and $ITMH^{lo}$, confirming the intrinsic transcriptional heterogeneity of intra-tumoral malignant cells (Supplementary Fig. 1e–f). We also performed pseudotime trajectory analysis using Monocle and observed a tumor cell evolutionary trend from ITMHlo tumor cells to ITMHhi tumor cells (Fig. 1h) .

Single-cell analysis of ITMH-defined tumor cell-intrinsic UM subtypes with different clinical phenotypes and outcomes

We conducted differential expression analysis of malignant cells between $ITMH^{hi}$ and $ITMH^{lo}$ tumors to identify expression signatures related to malignant cell heterogeneity (Fig. 2a, Supplementary Table 1). 120 ITMH-related DEGs were identified, consisting of 78 $ITMH^{hi}$-specific genes and 42 $ITMH^{lo}$-specific

(See figure on next page.)

Fig. 1 ScRNA-seq analysis revealed transcriptional diversity of malignant cells within and between UM tumors. **a** t-SNE visualization of 51464 cells from 17 UM patients, colored by clusters. **b** Dot plot of representative cell markers among each cluster; dot size represents abundance, and color represents expression level. **c** t-SNE visualization of 51464 cells from 17 UM patients, colored by main cell types. **d** Heatmap of Spearman's correlations among each cluster. **e** t-SNE visualization of 37660 tumor cells from 17 UM patients, colored by clusters. **f** t-SNE visualization of 37660 tumor cells from 17 UM patients, colored by the patient. **g** Sankey diagram showing the association between malignant cell subclusters and UM patients. **h** Differentiation trajectory of tumor cells inferred by Monocle, and colored by pseudo time (top) and ITMH subtype (bottom)

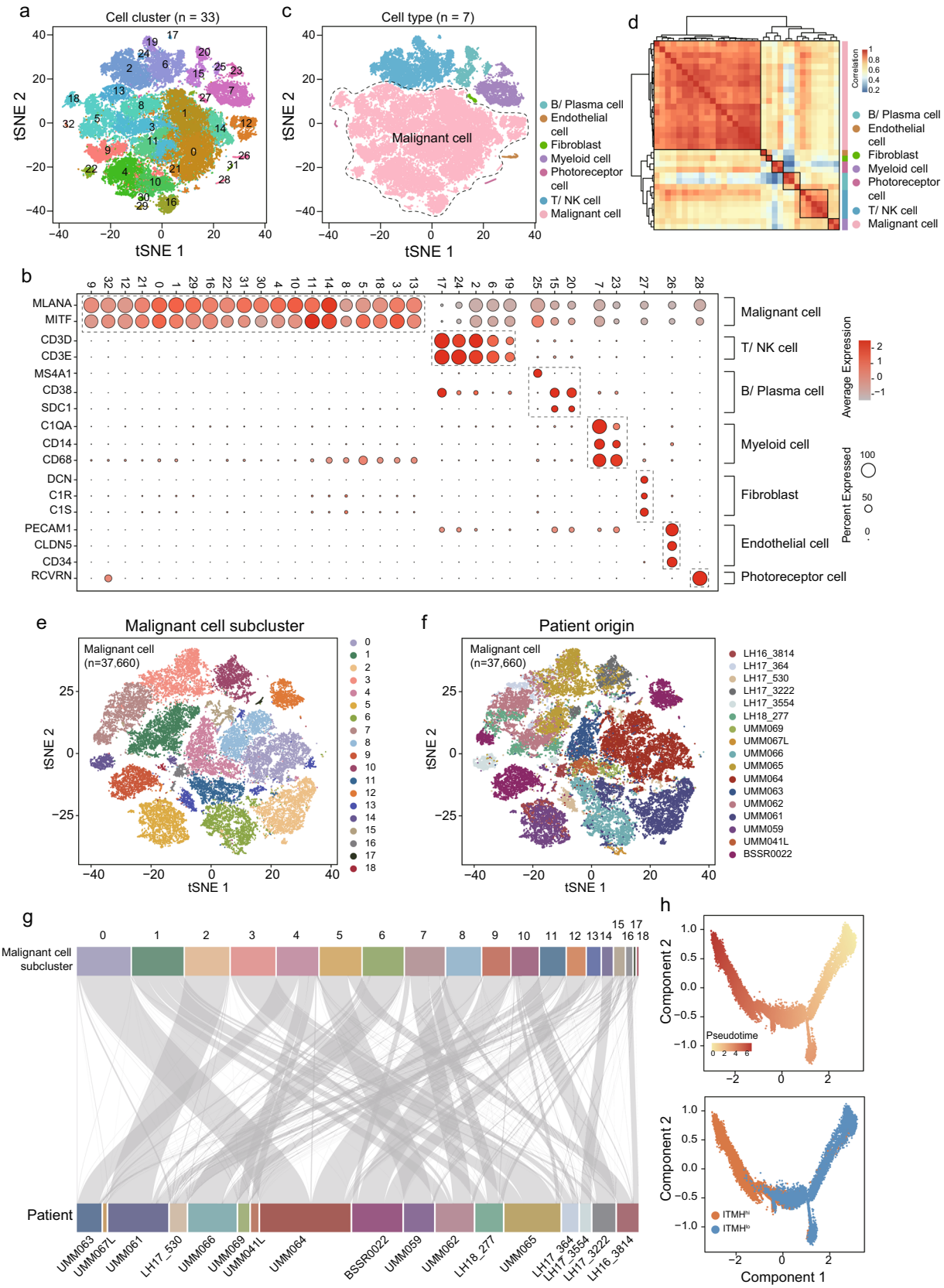

Fig. 1 (See legend on previous page.)

genes. Pathway enrichment analysis revealed that ITMH^{hi}-specific genes were overrepresented in pathways related to stress responses, Blood vessel morphogenesis, cell death and cell proliferation, whereas ITMH^{lo}-specific genes were predominantly enriched in cellular biosynthetic processes and aerobic respiration (Fig. 2b). To gain further insight into the metabolic alterations associated with increasing ITMH, we measured the level of enrichment for each metabolic pathway in KEGG. Our results revealed that oxidative phosphorylation and glycolysis were differentially upregulated in ITMH^{lo} and ITMH^{hi} tumors, respectively, indicating a marked shift in metabolic profiles (Supplementary Fig. 2a). We then applied our data to bulk tissue cohorts and observed a negative correlation between the expression of ITMH^{hi}-specific genes and that of ITMH^{lo}-specific genes in UM patients, indicating the existence of highly variable intra-tumoral malignant cell heterogeneity (Supplementary Fig. 2b).

We then evaluated the scaled t-test statistic values of the expression levels of ITMH-related genes in each patient as the ITMH score, categorizing UM patients into two distinct ITMH subtypes. Specifically, the ITMH^{hi} subtype (n = 43, ITMH score > 0) comprised of highly heterogeneous malignant cells characterized by high expression of ITMH^{hi}-specific gene signature and low expression of ITMH^{lo}-specific gene signatures, whereas the ITMH^{lo} subtype (n = 37, ITMH score < 0) was composed of malignant cells with low heterogeneity characterized by high expression of ITMH^{lo}-specific gene signature and low expression of ITMH^{hi}-specific gene signatures (Fig. 2c). Finally, we investigated the impact of transcriptional heterogeneity on patient outcome and found that both overall survival (OS) and progression-free survival (PFS) were significantly worse in patients with the ITMH^{hi} subtype than in those with the ITMH^{lo} subtype (HR = 10.94, 95% CI 10.32–11.57, p = 0.00013 for OS and HR = 52, 95% CI 21–130, p = 0.0018 for PFS, Fig. 2d, Supplementary Fig. 2c). Additionally, we verified our findings in an additional cohort (Laurent's cohort), in which 63 patients were stratified into ITMH^{hi} and ITMH^{lo} subtypes, and significant differences in overall survival were observed (HR = 2.82, 95% CI 2.47–3.18, p = 0.0016) (Fig. 2e-f). Finally, multivariate Cox regression analysis demonstrated that ITMH classification and ITMH score were reliable predictors of survival, independent of clinical/histopathological variables (ITMH classification: ITMH^{hi} versus ITMH^{lo}: HR = 3.4, 95% CI 1.1–11, p = 0.037 for TCGA-UM cohort; HR = 3.7, 95% CI 1.4–10, p = 0.0085 for Laurent's cohort; ITMH score: HR = 2.2, 95% CI 1.2–3.9, p = 0.011 for TCGA-UM cohort; HR = 1.8, 95% CI 1.1–2.9, p = 0.014 for Laurent's cohort) (Fig. 2g, Supplementary Fig. 2d). We next investigated the association between ITMH subtypes and previously defined GEP class as well as SCNA cluster. Our results demonstrated that UM patients from different GEP classes or SCNA clusters could be further classified into different ITMH subtypes, and we found a clear survival difference between ITMH^{hi} and ITMH^{lo} patients within GEP class 2 patients (median survival 29.1 months vs. 46.5 months), indicating that our ITMH subtypes can further stratify risk for previously defined subtypes (Fig. 2h, Supplementary Fig. 2e). Collectively, single-cell and bulk data analyses showed the clinical relevance of intra-tumoral malignant cell transcriptional heterogeneity with patient prognosis. The single-cell expression signature of malignant cell heterogeneity can robustly identify malignant cell-intrinsic subtypes from bulk tumor transcriptomes.

Molecular characteristics correlated with intra-tumoral malignant cell heterogeneity

To investigate whether the genomic features of malignant cells differed between ITMH^{hi} and ITMH^{lo} tumors, we analyzed the inferred CNVs for each malignant cell at the single-cell level. We found that genomic heterogeneity, calculated from inferred CNVs, was significantly associated with transcriptomic heterogeneity, with greater genomic instability observed in malignant cells from ITMH^{hi} tumors (Supplementary Fig. 3a). In addition, we observed frequent deletions of chromosome 3 and gains of chromosome 8 in malignant cells from ITMH^{hi} tumors compared to those from ITMH^{lo} tumors (Fig. 3a).

(See figure on next page.)

Fig. 2 Single-cell analysis defined tumor cell-intrinsic UM subtypes with different clinical phenotypes and patient outcomes. **a** Volcano plots showing the differentially expressed genes (DEGs) of malignant cells between ITMH^{hi} and ITMH^{lo} tumors. **b** Visualization of functionally categorized networks with enriched Gene Ontology (GO) terms as nodes, the node size denotes the enrichment significance. **c** Heatmap showing the relative expression of ITMH^{hi}-specific genes and ITMH^{lo}-specific genes in the TCGA-UM cohort. The landscape of clinical characteristics among different subtypes is shown at the top. **d** Kaplan–Meier survival plot of overall survival between two ITMH subtypes in the TCGA-UM cohort. Statistical difference was calculated by log-rank test. **e** Heatmap showing the relative expression of ITMH^{hi}-specific genes and ITMH^{lo}-specific genes in Laurent's cohort. **f** The Kaplan–Meier overall survival plot between ITMH subtypes in Laurent's cohort. Statistical difference was calculated by log-rank test. **g** Forest plots showing hazard ratio (HR) with 95% confidence intervals (CI) and p-values calculated by Cox regression analyses in multivariate analyses adjusted for clinical characteristics in TCGA and Laurent's cohorts. **h** Sankey diagram showingthe association between ITMH subtypes and previously defined molecular subtypes

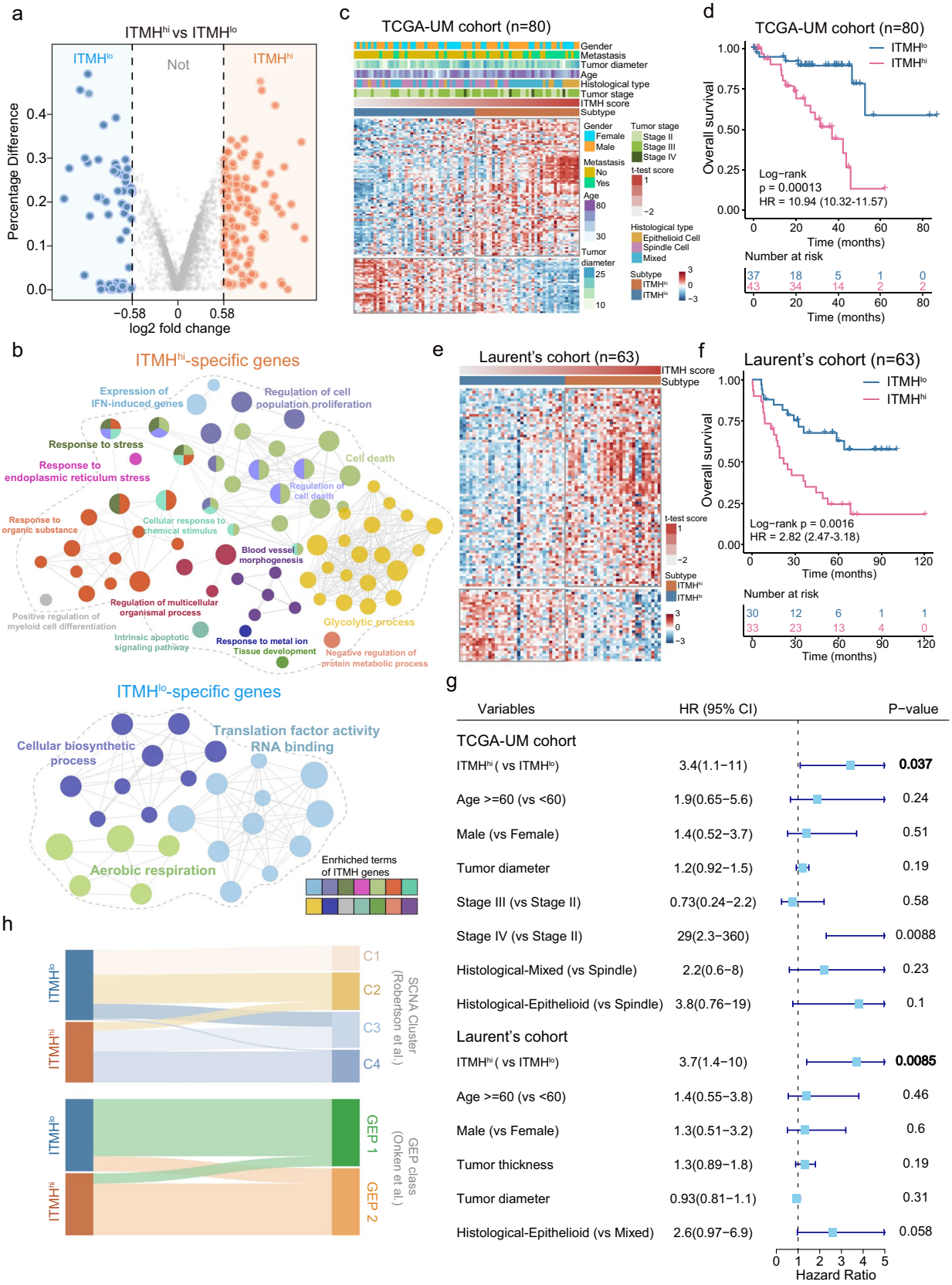

Fig. 2 (See legend on previous page.)

Further validation analysis was performed in an independent TCGA-UM cohort, which revealed that ITMH^{hi} patients were associated with a higher proportion of genome altered (FGA) (Supplementary Fig. 3b). Compared to ITMH^{lo} patients, copy loss of chromosomes 3, 6q, 8p and 16q, and copy gain of chromosomes 4p and 8q were observed in ITMH^{hi} patients (Fig. 3b). Gene-level analysis showed the enrichment of ITMH^{hi}-specific genes identified from scRNA-seq in chromosome 8q (Fig. 3b), suggesting that the transcriptomic features of tumor cells in ITMH^{hi} tumors may be partly due to copy gain of chromosome 8q. GISTIC analysis identified a prominent loss peak at 3q28, which included several known GEP class 2 downregulated signatures (*FXR1, EIF1B, ROBO1, LMCD1, SATB1*) and *BAP1*, a gene previously shown to facilitate suppressive immune responses [34–36]. As genomic mutations in tumors have been strongly associated with intra-tumoral malignant cell heterogeneity [37], we illustrated the landscape of commonly mutated genes between ITMH^{lo} and ITMH^{hi} patients (Fig. 3c). *SF3B1*, *EIF1AX* and *SF3B3* were frequently mutated in ITMH^{lo} patients and were previously associated with improved survival and reduced metastatic risk [38, 39]. In contrast, five significantly mutated genes were identified in ITMH^{hi} patients, including *CYSLTR2* and *TYRO3*, which have been implicated in tumorigenesis, tumor cell survival, proliferation, and metastasis in several cancers [40, 41]. These results suggest that ITMH in UM is significantly associated with aberrant genomic aberrations.

To gain deeper insights into the transcriptomic programs associated with intra-tumoral malignant cell heterogeneity, we used consensus non-negative matrix factorization (NMF) to identify coherent gene sets preferentially co-expressed by individual cells across 17 tumors in the scRNA-seq cohort. This analysis yielded 88 gene signatures, which were subjected to hierarchical clustering to reveal five distinct transcriptomic programs with discrete biological functions (Fig. 3d). Program-1 was involved in oxidative phosphorylation (*UQCRQ, NDUFA4, COX6C*), and program-2 was characterized by immediate early genes (*FOSB*, *JUNB*, *FOS*), activated by different stimuli and stress responses. Program-3 was enriched in mitochondrial genes, while program-4 was associated with immune response, with upregulation of MHC genes (*HLA-A*, *HLA-B*, *HLA-C*). Program-5 included hypoxia-related genes (*GAPDH*, *LDHA*, *ENO1*) and may be hypoxia-dependent (Fig. 3e). We further quantified the program activity in each UM tumor by calculating the program enrichment scores, and examined the dependency between transcriptomic programs and heterogeneity of intra-tumoral malignant cells. We observed a strong association between stress (program-2) and immune response (program-4) in ITMH^{hi} tumors, while ITMH^{lo} tumors displayed characteristics of a mitochondrial-enriched program (program-3) (Fig. 3f). These findings were confirmed in the TCGA-UM cohort, where ITMH^{hi} patients showed significantly higher program scores of program-2 and program-4, and ITMH^{lo} patients showed enhanced program-3 scores (Fig. 3g).

Relationship of intra-tumoral malignant cell heterogeneity with immune microenvironment reprogramming

To assess whether the heterogeneity of intra-tumoral malignant cells could reshape the immune-associated characteristics and cell composition within the TME, we performed a detailed analysis of immune cell types, including T/NK cells, myeloid cells, and B/plasma cells in UM. We re-clustered and identified five distinct subsets of T/NK cells (CD4 T, CD8 Tex, Prol Tex, NK and Treg), three subsets of myeloid cells (TAM, monocytes and DC) and two cell subsets of B/plasma (Fig. 4a, Supplementary Fig. 4a).

Our analysis revealed that the differences in the immune microenvironment between ITMH^{lo} and ITMH^{hi} tumors were mainly derived from infiltrating changes in T cells. As shown in Fig. 4b, ITMH^{hi} tumors exhibited higher infiltration of CD8 Tex, Prol Tex and Treg cells, with increased levels of exhaustion and immunosuppression scores (Fig. 4b, c), indicating a highly immunosuppressed tumor microenvironment with weak T cell-mediated killing capacity in ITMH^{hi} tumors. In contrast, TAM infiltration levels did not differ significantly between the two subtypes, but their functions and characteristics were altered. We

(See figure on next page.)

Fig. 3 Molecular characteristics correlated with malignant cell heterogeneity. **a** The landscape of large-scale copy number variations (CNVs) in the single-cell cohort inferred by inferCNV. **b** The landscape of large-scale copy number variations (CNVs) in the TCGA-UM cohort is shown at the top, the distribution of ITMH^{hi} and ITMH^{lo}-specific genes in the chromosome locus is shown in the middle, the GISTIC analysis of copy number gain and loss of ITMH^{hi} and ITMH^{lo} tumors are shown at the bottom. **c** The landscape of frequently mutated genes between ITMH^{hi} and ITMH^{lo} tumors, respectively. **d** Heatmap showing the correlation of all 88 signatures determined from the cNMF algorithm, 5 highly correlated expression programs are highlighted. **e** Top enriched pathways of 5 tumor expression programs. **f** Spearman correlation between diversity score and enrichment score of 5 tumor expression programs. **g** Box plots showing the differences in program score between two subtypes in the TCGA-UM cohort; each box indicates the interquartile range between the 25th and 75th percentiles. Statistical difference was calculated by the Wilcoxon rank-sum test

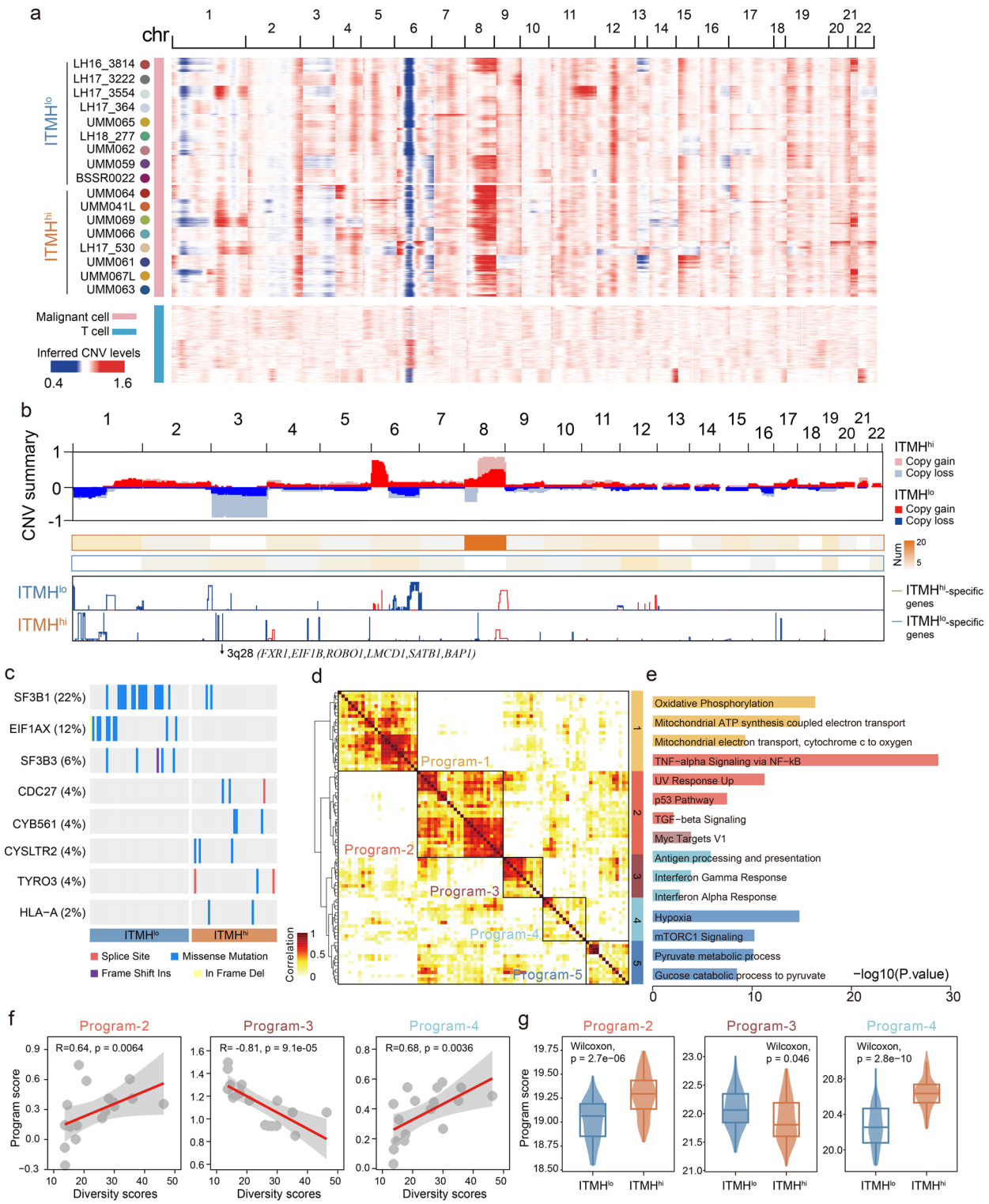

Fig. 3 (See legend on previous page.)

observed enrichment of glycolysis and cell adhesion molecules in ITMH^{hi} tumors, suggesting metabolic activation and reduced TNFa signaling via nfkb, cytokine receptor interaction and toll-like receptor signaling pathways, which are associated with inflammation and innate immune responses (Supplementary

Fig. 4b). To validate our findings, we performed computational immune composition estimation using CIBERSORT and ssGSEA on the TCGA bulk transcriptome data, which confirmed the enrichment of these T cell subsets (Fig. 4d).

We used the SCENIC method to identify the key transcription factor (TF) responsible for inducing the reprogramming of T cell phenotypes in ITMH^{hi} tumors. Our results revealed that ITMH^{hi}-derived T cells exhibited activated signal transducer and activator of transcription 1 (*STAT1*), with significant upregulation in Treg, CD8 Tex, and Prol Tex (Fig. 4e). Aberrant activation of STAT1 has been identified in several human cancers, demonstrating its ability to upregulate numerous cytokines and chemokines and contribute to an immunosuppressive TME [42–44]. It can, therefore, be inferred that reprogramming of STAT1 induces the immunosuppressive TME observed in the ITMH^{hi} subtype. To further investigate intercellular interactions in the immune microenvironment, we inferred putative cell-to-cell interactions based on ligand-receptor signaling from scRNA-seq data. We found that malignant cells from ITMH^{hi} tumors exhibited more outgoing interactions than those from ITMH^{lo} tumors (Fig. 4f). We further used CellChat to investigate the interactions between malignant cells and other immune cells in the TME. We observed that malignant cells had strong relationships with T/NK cell subsets, especially NK, CD8 Tex, and Prol Tex. Additionally, we found that human leukocyte antigen (HLA) class I molecules secreted by malignant cells had more interactions with receptors (CD8A and CD8B) expressed on these three subsets in the TME of ITMH^{hi} tumors compared to ITMH^{lo} tumors (Fig. 4g, Supplementary Fig. 4c). And these HLA class I molecules showed significantly higher expression in malignant cells from ITMH^{hi} tumors (Supplementary Fig. 4d). These ligand-receptor pairs indicated a possible underlying immune escape mechanism and induced an immunosuppressive environment by affecting the antigen-presenting capacity in ITMH^{hi} tumors. Based on these findings, we defined the ITMH^{hi} subtype as the pro-tumoral subtype and the ITMH^{lo} subtype as the anti-tumoral subtype, reflecting their distinct roles in tumor behavior and immune features.

Generation and validation of a 9-gene signature for defining UM tumor cell-intrinsic subtypes and prognosticating survival

Given the well-established correlation between intratumoral malignant cell heterogeneity and patient prognosis, we sought to develop a clinically applicable gene expression signature for UM tumor cell-intrinsic subtype classification. Based on the DEGs obtained from single-cell analysis of malignant cells between ITMH^{hi} and ITMH^{lo} tumors, we conducted the multistep analyses described in Methods and generated a 9-gene signature in the TCGA-UM cohort (Fig. 5a). We then independently validated the 9-gene signature in three multicenter UM cohorts. Using bulk transcriptome data from RNA-sequencing or microarrays, the 9-gene signature was calculated for each tumor patient and assigned patients to either the ITMH^{hi} or ITMH^{lo} subtype. Survival analysis revealed that patients in the predicted ITMH^{hi} subtype had significantly shorter survival than those in the predicted ITMH^{lo} subtype (HR = 3.01, 95% CI 2.67–3.36, p = 0.00074 for Laurent's cohort; HR = 6.36, 95% CI 5.82–6.90, p = 0.00012 for Gangemi's cohort and HR = 11.98, 95% CI 11.19–12.78, p < 0.0001 for van Essen'scohort) (Fig. 5b). We also performed a comparative analysis of the 9-gene signature against existing cytogenetic and molecular classifiers in UM by comparing the ROC curves for 5-year survival. In the TCGA cohort, the 9-GS and GEP classes demonstrated excellent performance, outperforming Robertson's SCNA classes and cytogenetic classifiers. Given the lack of genomic data in the validation cohorts, we compared the 9-GS and GEP classes and revealed that the 9-GS showed superior performance, with higher AUC values, in both the Gangemi and van Essen cohorts (Supplementary Fig. 5).

Discussion

UM is a highly aggressive and heterogeneous cancer for which effective treatment options are currently limited, particularly in the metastatic setting. Previous studies using multi-omics approaches have

(See figure on next page.)

Fig. 4 Relationship of malignant cell heterogeneity with immune microenvironment reprogramming. **a** t-SNE visualization of T, myeloid, and B cells, colored by cell subsets. CD8 Tex: exhausted CD8 + T cells; Prol Tex: proliferative exhausted cells; TAM: tumor-associated macrophages; DC: Dendritic cell. **b** Box plots showing the differences in the infiltrating proportion of CD8 Tex, Prol Tex and Treg between ITMH^{hi} and ITMH^{lo} tumors in single-cell cohort. **c** Box plots showing the differences in the exhaustion, immunosuppression, and cytotoxicity score between ITMH^{hi} and ITMH^{lo} tumors in the single-cell cohort. **d** Heatmap showing the infiltrating immune composition using CIBERSORT and ssGSEA. **e** Heatmap showing the relative activity of transcription factor in T cell subsets. **f** Scatter plot showing the outgoing and incoming interaction strength of each cell subset in ITMH^{lo} tumors and ITMH^{hi} tumors. **g** Dot plot of ligand-receptor interaction from tumor cells to immune cells between ITMH^{hi} tumors and ITMH^{lo} tumors; dot size represents the P-value, and color represents the interaction strength

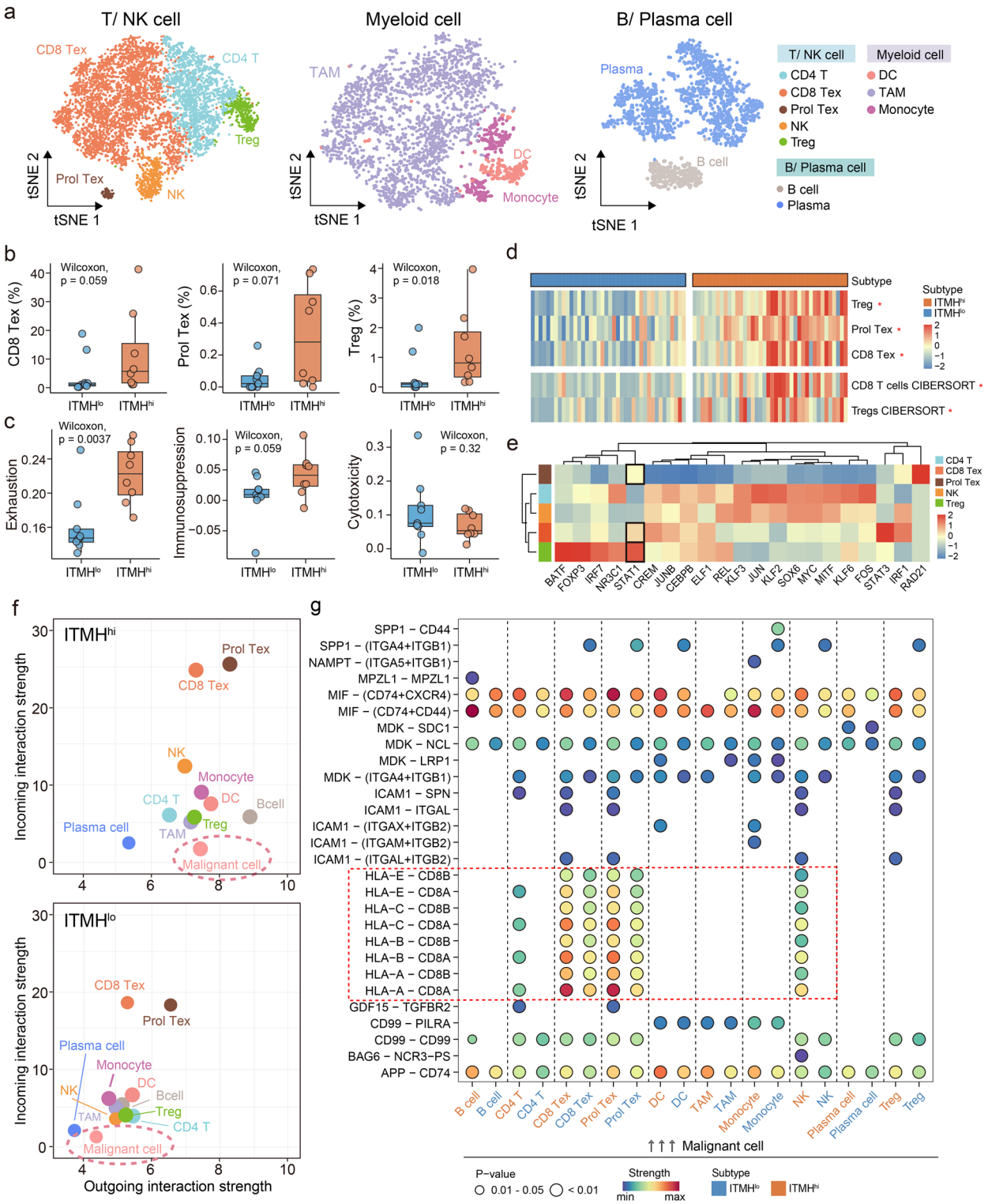

Fig. 4 (See legend on previous page.)

identified intertumoral molecular heterogeneity based on population-level data [45]. ITH has been recognized as a cancer hallmark and has contributed to tumor evolution, disease progression, and therapy resistance [46]. Although scRNA-seq analyses have been used to characterize tumor ecosystems and the

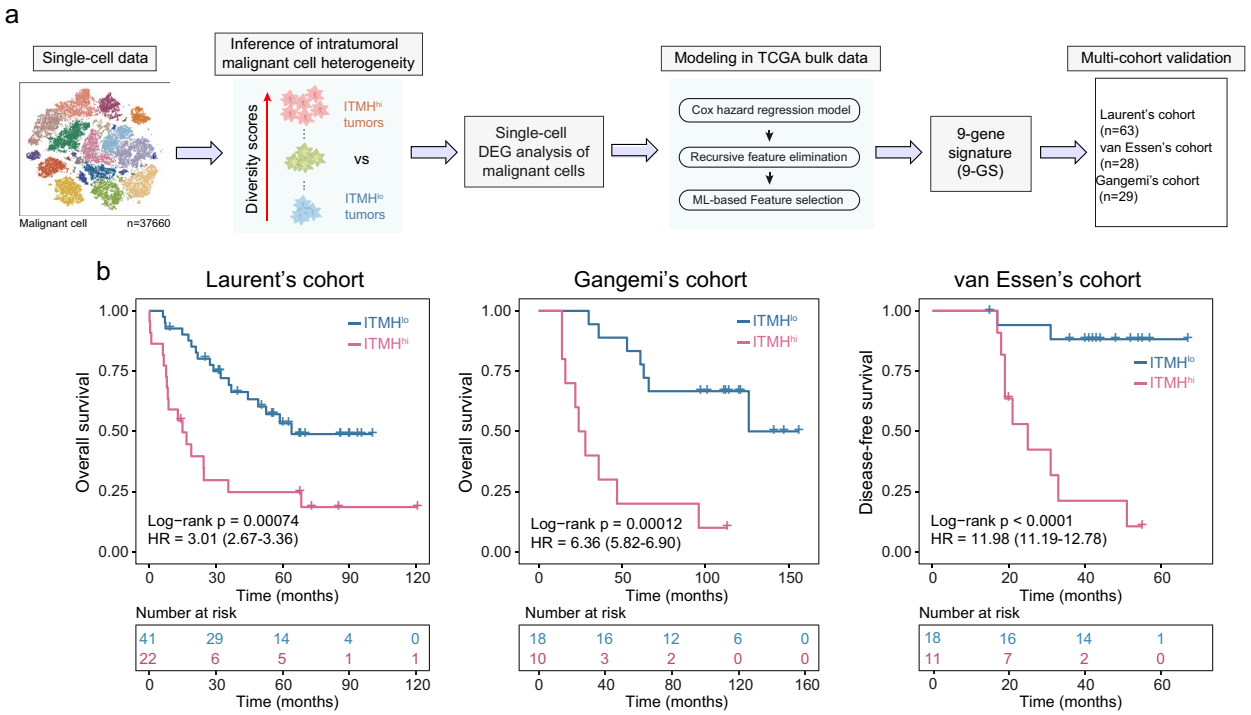

Fig. 5 Generation and validation of a 9-gene signature for defining UM tumor cell-intrinsic subtypes and prognosticating survival. **a** Schematic representation of feature selection and model construction. **b** Kaplan–Meier survival plot of overall survival or disease-free survival between predicted ITMH^{hi} patients and non-predicted ITMH^{lo} patients in three public UM cohorts. Statistical difference was calculated by log-rank test

microenvironment of UM [19, 20, 47], a more comprehensive understanding of the underlying biodiversity and heterogeneity of UM malignant cells at the single-cell level is still lacking. In this study, we performed a comprehensive integrated scRNA-seq analysis of 37,660 UM malignant cells from 17 patients, which revealed the transcriptional diversity and heterogeneity of UM malignant cells at the single-cell resolution. Furthermore, these transcriptomically distinct malignant cell subpopulations represented intertumoral and intratumoral heterogeneity.

We revealed that the malignant cells in UM undergo progressive changes from low ITMH to high ITMH, which are accompanied by alterations in functional programs and metabolic patterns. Notably, we identified five common expression programs that recur across transcriptomically distinct malignant cell subpopulations from scRNA-seq data, suggesting that the gene signatures of these five programs are predominantly expressed in most UM malignant cells and are crucial in determining the biology and phenotypes of UM malignant cells, including their abilities to survive, proliferate, migrate and metastasize. However, only three programs (stress responses, MYC, and antigen presentation) significantly differed and were associated with the tumor cell composition diversity of individual tumors. These findings suggest the functional specialization of different malignant cell subpopulations that may contribute to tumor progression, metastasis, and patient prognosis in UM. Moreover, UM tumors with different ITMH subtypes exhibited distinct metabolic phenotypes for energy production. ITMH^{lo} tumors showed enrichment in oxidative phosphorylation, suggesting that clinical treatments for this subtype of patients may be more suitable for targeting mitochondrial function or oxidative phosphorylation pathways. In contrast, ITMH^{hi} tumors exhibited an up-regulation of glycolysis function, indicating that these patients may benefit from treatment strategies targeting the glycolysis pathway, such as glycolysis-targeting or carbohydrate restriction. This metabolic switch from OXPHOS to glycolysis has been reported to be closely associated with the regulation of oncogenes in tumorigenesis and to promote an immunosuppressive microenvironment in cancers [48]. Given the highly immunosuppressive TME of ITMH^{hi} patients, characterized by an enrichment of exhausted T cells and Tregs and a depletion of cytotoxicity scores, treatment regimens with immune checkpoint inhibitors or other immunomodulatory drugs may be considered to restore immune activity for these patients. Heterogeneity in functional programs, metabolic pattern and immune

microenvironment of different ITMH tumors enabled us to gain insight into the evolutionary mechanisms of malignant cells in UM and to develop more effective methods for cancer intervention.

Considerable efforts have been made to investigate tumor cell heterogeneity in various cancer types, such as liver cancer [13] and gastric adenocarcinoma [14], and to identify functional programs and gene expression signatures associated with tumor progression, drug resistance or metastasis [49–51]. The observed effects of ITH on tumor subtypes and patient prognosis highlight the importance of investigating the underlying cellular phenotypes and heterogeneity. Although tumor ecosystem diversity in the tumor microenvironment influences tumor subtype heterogeneity [52–54], ITH in UM at the single-cell level remains largely unknown. Although two recent RNA-seq studies have made initial attempts to reveal intra-tumoral cellular heterogeneity in UM tumors [19, 20], there is still a knowledge gap regarding the impact of malignant cell ITH on tumor characteristics and subtype classification at both single-cell and bulk levels. Although multi-omic characterization of UM has identified molecularly and clinically distinct subtypes at the bulk level [45, 55–57], increasing evidence from scRNA-seq studies suggests a refinement of subtype classification beyond the current bulk-based subtypes [16, 58, 59]. However, accurate classification and characterization of UM subtypes at the single-cell resolution remains to be achieved. Therefore, we quantified gene signatures of tumor cell diversity within tumors based on bulk transcriptomes across different UM datasets and identified two tumor cell-intrinsic cellular subtypes ($ITMH^{hi}$ and $ITMH^{lo}$). Consistent with the previously observed association between tumor cell diversity and patient survival in other cancer types [13, 14], patients with different levels and diversity of malignant cell composition differed in their survival outcomes, with $ITMH^{hi}$ associated with poorer outcomes and $ITMH^{lo}$ with better outcomes. Furthermore, tumor cell-intrinsic cellular subtypes are prognostic independent of clinical and histopathological features but also provide a further substratification beyond the current subtypes by highlighting molecular, biological and immune microenvironment features underlying these two tumor-cell-intrinsic cellular subtypes. These findings provide important directions for future clinical trials and treatment decisions in UM.

The accurate delineation of UM subtypes is essential for developing effective clinical treatment strategies. Identifying tumor cell-intrinsic subtypes offers new insights into the admixture of established molecular subtypes within UM. To translate single-cell-defined tumor-cell-intrinsic subtypes into clinical practice with bulk data, we developed a 9-gene expression signature to classify UM tumor-cell-intrinsic subtypes. The 9-gene expression signature showed high prognostic accuracy in several multicenter UM patient cohorts. With standard chemotherapeutic agents, drug resistance in UM patients has become a critical challenge. Although currently used, preclinical drug screening with cell lines and xenograft models poorly reflects the complex molecular landscape of UM [6].

Conclusions

Our study uncovered the transcriptomic landscape of UM tumor cells, revealing the transcriptional diversity and heterogeneity among malignant cells through integrated single-cell RNA-seq and bulk transcriptome analyses. By leveraging the heterogeneous gene expression programs of malignant cells, we identified tumor cell-intrinsic subtypes of UM with distinct molecular, biological, and clinical features. Furthermore, we established and validated a 9-gene signature to translate scRNA-seq information into bulk tissue transcriptome for clinical application in patient stratification beyond the previously established consensus molecular subtype classification of UM. In conclusion, our study provides insight into understanding the intra-tumoral heterogeneity of UM and its potential impact on patient stratification.

Abbreviations

UM	Uveal melanoma
ITH	Intra-tumoral heterogeneity
scRNA-seq	Single-cell RNA sequencing
t-SNE	T-distributed stochastic neighbourhood embedding
CNV	Copy-number variation
TF	Transcription factor

Supplementary Information

The online version contains supplementary material available at https://doi.org/10.1186/s12967-024-05831-2.

Additional file 1: Supplementary Figures.

Additional file 2: Supplementary Table 1.

Author contributions

MZ, JS conceived and designed the study. KL, JZH and YT performed data analysis and interpretation. KL wrote the first draft. MZ and JS revised the manuscript. All authors read and approved the final manuscript.

Funding

This study was supported by the National Natural Science Foundation of China (62372331). The funders had no roles in study design, data collection and analysis, publication decision, or manuscript preparation.

Availability of data and materials

All public single-cell RNA sequencing data and bulk microarray data are available from the GEO database under accession numbers GSE139829, GSE138665, GSE22138, GSE27831 and GSE84976. Bulk RNA-seq data were obtained from UCSC Xena (GDC TCGA-UM cohort) (https://xenabrowser.net/datapages/). The code generated or used during the study are available in GitHub (https://github.com/ZhoulabCPH/UVM_ITH).

Declarations

Ethics approval and consent to participate
Not applicable.

Consent for publication
Not applicable.

Competing interests
The authors declare no competing financial interests.

Received: 29 August 2024 Accepted: 30 October 2024
Published online: 12 November 2024

References

1. Smit KN, Jager MJ, de Klein A, Kili E. Uveal melanoma: towards a molecular understanding. Prog Retin Eye Res. 2020;75: 100800.
2. Shain AH, Bagger MM, Yu R, Chang D, Liu S, Vemula S, et al. The genetic evolution of metastatic uveal melanoma. Nat Genet. 2019;51(7):1123–30.
3. Kaliki S, Shields CL. Uveal melanoma: relatively rare but deadly cancer. Eye (Lond). 2017;31(2):241–57.
4. Nathan P, Hassel JC, Rutkowski P, Baurain JF, Butler MO, Schlaak M, et al. Overall survival benefit with tebentafusp in metastatic uveal melanoma. N Engl J Med. 2021;385(13):1196–206.
5. Lin W, Beasley AB, Ardakani NM, Denisenko E, Calapre L, Jones M, et al. Intra- and intertumoral heterogeneity of liver metastases in a patient with uveal melanoma revealed by single-cell RNA sequencing. Cold Spring Harb Mol Case Stud. 2021. https://doi.org/10.1101/mcs.a006111.
6. Jager MJ, Shields CL, Cebulla CM, Abdel-Rahman MH, Grossniklaus HE, Stern MH, et al. Uveal melanoma. Nat Rev Dis Primers. 2020;6(1):24.
7. de Bruin EC, McGranahan N, Mitter R, Salm M, Wedge DC, Yates L, et al. Spatial and temporal diversity in genomic instability processes defines lung cancer evolution. Science. 2014;346(6206):251–6.
8. Greaves M. Evolutionary determinants of cancer. Cancer Discov. 2015;5(8):806–20.
9. Nguyen PHD, Ma S, Phua CZJ, Kaya NA, Lai HLH, Lim CJ, et al. Intratumoural immune heterogeneity as a hallmark of tumour evolution and progression in hepatocellular carcinoma. Nat Commun. 2021;12(1):227.
10. Dentro SC, Leshchiner I, Haase K, Tarabichi M, Wintersinger J, Deshwar AG, et al. Characterizing genetic intra-tumor heterogeneity across 2,658 human cancer genomes. Cell. 2021;184(8):2239-54 e39.
11. Li K, Zhang R, Wen F, Zhao Y, Meng F, Li Q, et al. Single-cell dissection of the multicellular ecosystem and molecular features underlying microvascular invasion in HCC. Hepatology. 2023. https://doi.org/10.1097/HEP.0000000000000673.
12. Hinohara K, Polyak K. Intratumoral heterogeneity: more than just mutations. Trends Cell Biol. 2019;29(7):569–79.
13. Ma L, Hernandez MO, Zhao Y, Mehta M, Tran B, Kelly M, et al. Tumor cell biodiversity drives microenvironmental reprogramming in liver cancer. Cancer Cell. 2019;36(4):418–306.
14. Wang R, Dang M, Harada K, Han G, Wang F, Pool Pizzi M, et al. Single-cell dissection of intratumoral heterogeneity and lineage diversity in metastatic gastric adenocarcinoma. Nat Med. 2021;27(1):141–51.
15. Yeo SK, Zhu X, Okamoto T, Hao M, Wang C, Lu P, et al. Single-cell RNA-sequencing reveals distinct patterns of cell state heterogeneity in mouse models of breast cancer. Elife. 2020. https://doi.org/10.7554/eLife.58810.
16. Joanito I, Wirapati P, Zhao N, Nawaz Z, Yeo G, Lee F, et al. Single-cell and bulk transcriptome sequencing identifies two epithelial tumor cell states and refines the consensus molecular classification of colorectal cancer. Nat Genet. 2022;54(7):963–75.
17. Lawson DA, Kessenbrock K, Davis RT, Pervolarakis N, Werb Z. Tumour heterogeneity and metastasis at single-cell resolution. Nat Cell Biol. 2018;20(12):1349–60.
18. McGranahan N, Swanton C. Clonal heterogeneity and tumor evolution: past, present, and the future. Cell. 2017;168(4):613–28.
19. Durante MA, Rodriguez DA, Kurtenbach S, Kuznetsov JN, Sanchez MI, Decatur CL, et al. Single-cell analysis reveals new evolutionary complexity in uveal melanoma. Nat Commun. 2020;11(1):496.
20. Pandiani C, Strub T, Nottet N, Cheli Y, Gambi G, Bille K, et al. Single-cell RNA sequencing reveals intratumoral heterogeneity in primary uveal melanomas and identifies HES6 as a driver of the metastatic disease. Cell Death Differ. 2021;28(6):1990–2000.
21. Hao Y, Hao S, Andersen-Nissen E, Mauck WM 3rd, Zheng S, Butler A, et al. Integrated analysis of multimodal single-cell data. Cell. 2021;184(13):3573–8729.
22. Korsunsky I, Millard N, Fan J, Slowikowski K, Zhang F, Wei K, et al. Fast, sensitive and accurate integration of single-cell data with Harmony. Nat Methods. 2019;16(12):1289–96.
23. Zheng Y, Chen Z, Han Y, Han L, Zou X, Zhou B, et al. Immune suppressive landscape in the human esophageal squamous cell carcinoma microenvironment. Nat Commun. 2020;11(1):6268.
24. Trapnell C, Cacchiarelli D, Grimsby J, Pokharel P, Li S, Morse M, et al. The dynamics and regulators of cell fate decisions are revealed by pseudotemporal ordering of single cells. Nat Biotechnol. 2014;32(4):381–6.
25. Aibar S, Gonzalez-Blas CB, Moerman T, Huynh-Thu VA, Imrichova H, Hulselmans G, et al. SCENIC: single-cell regulatory network inference and clustering. Nat Methods. 2017;14(11):1083–6.
26. Laurent C, Valet F, Planque N, Silveri L, Maacha S, Anezo O, et al. High PTP4A3 phosphatase expression correlates with metastatic risk in uveal melanoma patients. Cancer Res. 2011;71(3):666–74.
27. Gangemi R, Mirisola V, Barisione G, Fabbi M, Brizzolara A, Lanza F, et al. Mda-9/syntenin is expressed in uveal melanoma and correlates with metastatic progression. PLoS ONE. 2012;7(1): e29989.
28. van Essen TH, van Pelt SI, Bronkhorst IH, Versluis M, Nemati F, Laurent C, et al. Upregulation of HLA expression in primary uveal melanoma by infiltrating leukocytes. PLoS ONE. 2016;11(10): e0164292.
29. Mermel CH, Schumacher SE, Hill B, Meyerson ML, Beroukhim R, Getz G. GISTIC2.0 facilitates sensitive and confident localization of the targets of focal somatic copy-number alteration in human cancers. Genome Biol. 2011;12(4):41.
30. Thorvaldsdottir H, Robinson JT, Mesirov JP. Integrative genomics viewer (IGV): high-performance genomics data visualization and exploration. Brief Bioinform. 2013;14(2):178–92.
31. Gaujoux R, Seoighe C. A flexible R package for nonnegative matrix factorization. BMC Bioinformatics. 2010;11:367.
32. Jin S, Guerrero-Juarez CF, Zhang L, Chang I, Ramos R, Kuan CH, et al. Inference and analysis of cell-cell communication using cell chat. Nat Commun. 2021;12(1):1088.
33. Zeng D, Ye Z, Shen R, Yu G, Wu J, Xiong Y, et al. IOBR: multi-omics immuno-oncology biological research to decode tumor microenvironment and signatures. Front Immunol. 2021;12: 687975.
34. Harbour JW. A prognostic test to predict the risk of metastasis in uveal melanoma based on a 15-gene expression profile. Methods Mol Biol. 2014;1102:427–40.
35. Kalirai H, Dodson A, Faqir S, Damato BE, Coupland SE. Lack of BAP1 protein expression in uveal melanoma is associated with increased metastatic risk and has utility in routine prognostic testing. Br J Cancer. 2014;111(7):1373–80.
36. Koopmans AE, Verdijk RM, Brouwer RW, van den Bosch TP, van den Berg MM, Vaarwater J, et al. Clinical significance of immunohistochemistry for detection of BAP1 mutations in uveal melanoma. Mod Pathol. 2014;27(10):1321–30.
37. Sung JY, Shin HT, Sohn KA, Shin SY, Park WY, Joung JG. Assessment of intratumoral heterogeneity with mutations and gene expression profiles. PLoS ONE. 2019;14(7): e0219682.
38. Martin M, Masshofer L, Temming P, Rahmann S, Metz C, Bornfeld N, et al. Exome sequencing identifies recurrent somatic mutations in EIF1AX and SF3B1 in uveal melanoma with disomy 3. Nat Genet. 2013;45(8):933–6.
39. Yavuzyigitoglu S, Koopmans AE, Verdijk RM, Vaarwater J, Eussen B, van Bodegom A, et al. Uveal melanomas with SF3B1 mutations: a distinct subclass associated with late-onset metastases. Ophthalmology. 2016;123(5):1118–28.
40. Smart SK, Vasileiadi E, Wang X, DeRyckere D, Graham DK. The emerging role of TYRO3 as a therapeutic target in cancer. Cancers (Basel). 2018. https://doi.org/10.3390/cancers10120474.

41. Moore AR, Ceraudo E, Sher JJ, Guan Y, Shoushtari AN, Chang MT, et al. Recurrent activating mutations of G-protein-coupled receptor CYSLTR2 in uveal melanoma. Nat Genet. 2016;48(6):675–80.
42. Arzt L, Kothmaier H, Halbwedl I, Quehenberger F, Popper HH. Signal transducer and activator of transcription 1 (STAT1) acts like an oncogene in malignant pleural mesothelioma. Virchows Arch. 2014;465(1):79–88.
43. Greenwood C, Metodieva G, Al-Janabi K, Lausen B, Alldridge L, Leng L, et al. Stat1 and CD74 overexpression is co-dependent and linked to increased invasion and lymph node metastasis in triple-negative breast cancer. J Proteomics. 2012;75(10):3031–40.
44. Zhang Y, Liu Z. STAT1 in cancer: friend or foe? Discov Med. 2017;24(130):19–29.
45. Robertson AG, Shih J, Yau C, Gibb EA, Oba J, Mungall KL, et al. Integrative analysis identifies four molecular and clinical subsets in uveal melanoma. Cancer Cell. 2018;33(1):151.
46. Vitale I, Shema E, Loi S, Galluzzi L. Intratumoral heterogeneity in cancer progression and response to immunotherapy. Nat Med. 2021;27(2):212–24.
47. Li K, Sun L, Wang Y, Cen Y, Zhao J, Liao Q, et al. Single-cell characterization of macrophages in uveal melanoma uncovers transcriptionally heterogeneous subsets conferring poor prognosis and aggressive behavior. Exp Mol Med. 2023;55(11):2433–44.
48. Zheng J. Energy metabolism of cancer: Glycolysis versus oxidative phosphorylation (Review). Oncol Lett. 2012;4(6):1151–7.
49. Biermann J, Melms JC, Amin AD, Wang Y, Caprio LA, Karz A, et al. Dissecting the treatment-naive ecosystem of human melanoma brain metastasis. Cell. 2022;185(14):2591-608 e30.
50. Pozniak J, Pedri D, Landeloos E, Van Herck Y, Antoranz A, Vanwynsberghe L, et al. A TCF4-dependent gene regulatory network confers resistance to immunotherapy in melanoma. Cell. 2024;187(1):166-83 e25.
51. Tirosh I, Izar B, Prakadan SM, Wadsworth MH 2nd, Treacy D, Trombetta JJ, et al. Dissecting the multicellular ecosystem of metastatic melanoma by single-cell RNA-seq. Science. 2016;352(6282):189–96.
52. Barkley D, Moncada R, Pour M, Liberman DA, Dryg I, Werba G, et al. Cancer cell states recur across tumor types and form specific interactions with the tumor microenvironment. Nat Genet. 2022;54(8):1192–201.
53. Ge G, Han Y, Zhang J, Li X, Liu X, Gong Y, et al. Single-cell RNA-seq reveals a developmental hierarchy super-imposed over subclonal evolution in the cellular ecosystem of prostate cancer. Adv Sci (Weinh). 2022;9(15): e2105530.
54. Steen CB, Luca BA, Esfahani MS, Azizi A, Sworder BJ, Nabet BY, et al. The landscape of tumor cell states and ecosystems in diffuse large B cell lymphoma. Cancer Cell. 2021;39(10):1422–3710.
55. Cassoux N, Rodrigues MJ, Plancher C, Asselain B, Levy-Gabriel C, Lumbroso-Le Rouic L, et al. Genome-wide profiling is a clinically relevant and affordable prognostic test in posterior uveal melanoma. Br J Ophthalmol. 2014;98(6):769–74.
56. Onken MD, Worley LA, Ehlers JP, Harbour JW. Gene expression profiling in uveal melanoma reveals two molecular classes and predicts metastatic death. Cancer Res. 2004;64(20):7205–9.
57. Yan C, Hu X, Liu X, Zhao J, Le Z, Feng J, et al. Upregulation of SLC12A3 and SLC12A9 mediated by the HCP5/miR-140-5p Axis confers aggressiveness and unfavorable prognosis in uveal melanoma. Lab Invest. 2023;103(3): 100022.
58. Olbrecht S, Busschaert P, Qian J, Vanderstichele A, Loverix L, Van Gorp T, et al. High-grade serous tubo-ovarian cancer refined with single-cell RNA sequencing: specific cell subtypes influence survival and determine molecular subtype classification. Genome Med. 2021;13(1):111.
59. Li Q, Wang R, Yang Z, Li W, Yang J, Wang Z, et al. Molecular profiling of human non-small cell lung cancer by single-cell RNA-seq. Genome Med. 2022;14(1):87.

Publisher's Note